Available online at www.sciencedirect.com
SCIENCE DIRECT®
Chaos, Solitons and Fractals 27 (2006) 1239–1255
CHAOS SOLITONS & FRACTALS
www.elsevier.com/locate/chaos

Dynamics of modified Leslie–Gower-type prey–predator model with seasonally varying parameters

Sunita Gakkhar *, Brahampal Singh

Department of Mathematics, Indian Institute of Technology, Roorkee 247 667 (Uttranchal), India

Accepted 14 April 2005

Abstract

A modified Leslie–Gower-type prey–predator model composed of a logistic prey with Holling's type II functional response is studied. The axial point $(1,0)$ is found to be globally asymptotically stable in a domain. Condition for stability of the non-trivial equilibrium point is obtained. The existence of stable limit cycle of the system is also established. The analysis for Hopf bifurcation is carried out. The numerical simulations are carried out to study the effects of seasonally varying parameters of the model. The system shows the rich dynamic behavior including bifurcation and chaos.

1. Introduction

The study of ecological systems driven by periodic external forces is of considerable importance since the population communities are imbedded in seasonally varying environments. Due to seasonality, one or more of the model parameters may be affected. The intrinsic growth rates as well as the carrying capacities of one or more species are reported to be varying periodically in the presence of seasonal variations. In the absence of seasonal variations, the underlying autonomous nonlinear system for two interacting species can have limited dynamical behavior. However due to such variations, the two-dimensional non-autonomous systems are reported to have complex dynamical behavior [1–4].

In this paper the modified Leslie–Gower type prey–predator model, composed of a logistic prey with Holling's type II functional response is investigated. Asynchronous seasonal variations are considered simultaneously in different parameters. The seasonality is considered in the growth rate of the prey and the predator.

2. The Model

Consider a prey–predator system consisting of prey having density as X_1 and predators having density X_2. The predator is assumed to be sexually reproducing species in which mating frequency is directly proportional to the number of males as well as females. The following Leislie–Gower-type model [5,6] is used to represent the dynamics of prey–predator system:

* Corresponding author.
E-mail addresses: sungkfma@iitr.ernet.in, bps75dma@iitr.ernet.in (S. Gakkhar).

0960-0779/$ - see front matter © 2005 Elsevier Ltd. All rights reserved.
doi:10.1016/j.chaos.2005.04.097

$$\begin{aligned} dX_1/dT &= r_1' X_1(1-(X_1/K')) - \left(\frac{AX_1X_2}{1+BX_1}\right), \\ dX_2/dT &= r_2' X_2^2 - \frac{CX_2^2}{(DX_1+E)}, \\ X_1(0) &\geqslant 0 \quad \text{and} \quad X_2(0) \geqslant 0. \end{aligned} \tag{1}$$

The predator is consuming prey according to Holling type II functional response. The last term in the predator equation represents the loss in predator population due to rarity of its most favorite food X_1. The constant E normalizes the residual reduction in the predator population due to severe scarcity of its food. In the model r_1' and r_2' represent the intrinsic growth rates of two species, K' is the carrying capacity of prey in absence of predation, A is the search rate and B^{-1} is the half saturation constant.

We consider sinusoidal perturbations in periodic parameter $p(T)$ as

$$p'(T) = p(1+\varepsilon \sin \Omega T),$$

where p is the average value of p' and ε is the "degree" of seasonality; εp, is the magnitude of the perturbation and Ω is the angular frequency of the fluctuations caused by seasonality. Obviously $0 \leqslant \varepsilon \leqslant 1$ since p cannot be negative. $\varepsilon = 0$ corresponds to absence of seasonality, while $\varepsilon = 1$ means the maximum value of the parameter is twice its average value. In the model (1), intrinsic growth rates r_1' $(i = 1,2)$ are assumed to be periodically varying functions of time due to seasonal variations in the resources. Different biological species respond to seasonal variations quite differently, the two growth rates are assumed to vary asynchronously with the same period. It is further assumed that cause the seasonal variations in growth rate also affect the carrying capacity. It may be the abundance in the availability of food that may cause the increase in the growth of the species. The following periodic variations are assumed:

$$r_1' = r_1(1+\varepsilon_1 \sin(\Omega T)); \quad K' = K(1+\varepsilon_1 \sin(\Omega T)); \quad r_2' = r_2(1+\varepsilon_2 \sin(\Omega T+\phi)). \tag{2}$$

The phase angle ϕ lies between 0 *and* 2π.

The following non-dimensional variables and parameters reduce the number of model parameters from 8 to 4.

$$t = r_1 T, \quad x = X/K, \quad y = AX_2/r_1, \quad w_1 = BK, \quad w_2 = r_2/A, \quad w_3 = C/EA, \quad w_4 = DK/E.$$

Using (2) and the transformation $z = \theta t$ and $\theta = \Omega/r_1$, $\lambda = r_2\varepsilon_2/A$ in (1), we get the non-dimensional autonomous system as

$$\begin{aligned} dx/dt &= x(1-x) - (xy/(1+w_1x)) + \varepsilon_1 x \sin(z), \\ dy/dt &= w_2y^2 - (w_3y^2/(w_4x+1)) + \lambda y^2 \sin(z+\phi), \\ dz/dt &= \theta, \quad z(0) = 0. \end{aligned} \tag{3}$$

In the absence of seasonality, the non-dimensional form of the unforced system is obtained as

$$\begin{aligned} dx/dt &= x(1-x) - (xy/(1+w_1x)) = xf_1(x,y), \\ dy/dt &= w_2y^2 - (w_3y^2/(w_4x+1)) = yf_2(x,y). \end{aligned} \tag{4}$$

3. Analysis of corresponding unforced system

For biological feasibility of the model, the unforced system (4) must be Kolmogorov [7]. This is established in the Lemma 3.1.

Lemma 3.1. *In the domain* $D' = \{(x,y):\ 0 \leqslant x \leqslant \bar{x} \leqslant 1,\ 0 \leqslant y \leqslant \bar{y}\} \subset R_+^2$; *The system (4) is Kolmogorov for* $w_3/(1+w_4\bar{x})^2 < w_2 < w_3/(1+w_4\bar{x}) < w_3$.

The result of further analysis of unforced system (4) is given in the following theorems:

Theorem 3.2. *The Kolmogorov system (4) is uniformly bounded in the domain* D'.

$$D' = \{(x,y):\ 0 \leqslant x \leqslant \bar{x} \leqslant 1,\ 0 \leqslant y \leqslant \bar{y}\} \subset R_+^2.$$

Proof. Since $dx/dt \leqslant x(1-x)$ by usual comparison theorem implies that $\sup x \leqslant 1$ for sufficiently large $t > 0$.

Let $\eta(t) = x(t) + y(t)$

$$d\eta/dt = x(1-x) - (xy/(1+w_1x)) + y^2(w_2 - w_3/(1+w_4x))$$

or

$$d\eta/dt \leqslant x(1-x) + y^2(w_2 - w_3/(1+w_4\bar{x})) \quad \text{or} \quad d\eta/dt + \eta(t) \leqslant \beta, \tag{5}$$

where $\beta = \beta_1 + \beta_2$; $\beta_1 = \max\{x + x(1-x)\}$ and $\beta_2 = \max\{y + y^2(w_2 - w_3/(1+w_4\bar{x}))\}$. This shows the bounded ness of $\eta(t)$ implying the bounded ness of the system (4) in the domain $D' \subset R^2_+$.

Using inequality (5) and by usual comparison theorem for $t \geqslant 0$ we get

$$\eta(t) \leqslant \beta - (\beta - \eta(0))e^{-t}$$

For given $\varepsilon > 0$ there exists $t \geqslant T_1 \geqslant 0$ such that $x(t) \leqslant 1 + \varepsilon/2$, we have

$$\eta(t) \leqslant \beta - (\beta e^{T_1} - \eta(T_1)e^{T_1})e^{-t} \Rightarrow \eta(t) \leqslant \beta - (\beta - \eta(T_1)e^{T_1})e^{-t}$$

and then for all $t \geqslant T$ we have

$$\eta(t) \leqslant \beta + \frac{\varepsilon}{2} - \left(\beta + \frac{\varepsilon}{2} - \eta(T_1)e^{T_1}\right)e^{-t}.$$

Consider $T_2 \geqslant T_1$ such that

$$\left|\left(\beta + \frac{\varepsilon}{2} - \eta(T_1)e^{T_1}\right)\right|e^{-t} \leqslant \frac{\varepsilon}{2}.$$

$$\eta(t) \leqslant \beta + \varepsilon \text{ for all } t \geqslant T_2.$$

Then, we have

$$\operatorname{Sup}\eta(t) \leqslant \beta.$$

Therefore, the system is uniformly bounded and hence dissipative in positive quadrant D'. □

Since the solution is uniformly bounded and dissipative, it is concluded that the solution of the Kolmogorov system (4) is invariant in the domain D'.

There are three non-negative equilibrium points for the Kolmogorov system (4):

$$E_0 = (0,0), \quad E_1 = (1,0), \quad E_2 = (x^*, y^*); \quad x^* = (w_3 - w_2)/w_2w_4; \quad y^* = (1-x^*)(1+w_1x^*).$$

The equilibrium points E_0, E_1 exists and are the boundary point of the domain D'.

The variational matrices of system (4) about E_0 and E_1 are given by

$$V_0 = \begin{bmatrix} 1 & 0 \\ 0 & 0 \end{bmatrix} \quad \text{and} \quad V_1 = \begin{bmatrix} -1 & -(1+w_1)^{-1} \\ 0 & 0 \end{bmatrix}.$$

Thus, we get the unstable manifold about E_0 and stable manifold about E_1 along x axes. The equilibrium point E_1 is a saddle non-hyperbolic point.

Theorem 3.3. *The equilibrium point $E_1\{= (\bar{x}, 0) = (1,0)\}$ is globally stable in domain D' provided the following conditions are satisfied*:

$$\frac{w_1 - 1}{w_1} < \bar{x} < \frac{w_3 - w_2}{w_4w_2} \quad \text{and} \quad y < \left(\frac{1}{2l_1'w_2w_4} + \frac{\sqrt{A}\sqrt{2B}}{w_2w_4\sqrt{l_1'}\sqrt{l_2'}}\right)l_2',$$

where

$$l_1' = (1+w_1); \quad l_2' = (1+w_4),$$

$$A = (w_1\bar{x} + 1 - w_1) > 0; \quad B = (w_3 - w_2(w_4\bar{x} + 1)) > 0.$$

Proof. Consider the following positive definite function for arbitrarily chosen non-zero positive constants D_1 and D_2:$V(t) = D_1(u - \bar{x}\log(1 + \frac{u}{\bar{x}})) + D_2v^2$, $X = \bar{X} + u$, $y = v$ where u and v are the perturbation about the equilibrium point E_1.

$$\frac{dV}{dt} \leqslant -c_1^2u^2 - c_2^2v^2 - c_3uv + c_4uv^2,$$

where

$$c_1^2 = \frac{AD_1}{l_1}; \quad c_2^2 = \frac{2D_2B}{l_2}; \quad c_3 = \frac{D_1}{l_1}; \quad c_4 = \frac{2D_2w_2w_4}{l_2}; \quad l_1 = (1 + w_1x); \quad l_2 = (1 + w_4x),$$

$$A = (w_1\bar{x} + 1 - w_1) > 0; \quad B = (w_3 - w_2(w_4\bar{x} + 1)) > 0,$$

$$\frac{dV}{dt} < -c_1^2\left[u + \frac{c_3y - c_4y^2}{2c_1^2}\right]^2 - [4c_1^2c_2^2y^2 - (c_3y - c_4y^2)^2]/4c_1^2.$$

For V to be a Liapunov function, the expression $F = (c_3 - c_4y)^2 - 4c_1^2c_2^2$ must be negative.

It may be observed that $F = 0$ for $\mathbf{y} = \mathbf{y}_1 = \frac{\mathbf{c}_3+2\mathbf{c}_1\mathbf{c}_2}{\mathbf{c}_4}$ and $y = y_2 = \frac{c_3-2c_1c_2}{c_4}$.

Further dF/dy is positive for $y = \frac{c_3+2c_1c_2}{c_4}$. Therefore, F is negative for $y_2 < y < y_1$.

Choose the arbitrary constant $D_1 = 1$ and D_2 in such a manner that makes $y_2 < 0$. Thus, the equilibrium point is globally asymptotically stable in the domain $0 < y < y_1$. Substituting the values of c_1, c_2,c_3, c_4; the domain $0 < y < y_1$ is obtained as

$$y < \left(\frac{1}{2l_1'w_2w_4} + \frac{\sqrt{A}\sqrt{2B}}{w_2w_4\sqrt{l_1'}\sqrt{l_2'}}\right)l_2'.$$

For the following set of numerical data $w_1 = 0.6$, $w_2 = 0.2$, $w_3 = 8$, $w_4 = 0.1$, the equilibrium point E_1 is validated to be globally asymptotically stable as shown in Fig. 1 for distinct initial values. Note that x, y, z are plotted on y_1, y_2, y_3 axes. □

Theorem 3.4. *The unique non-zero positive equilibrium point E_2 is locally asymptotically stable provided the following condition is satisfied*

$$x^* > (w_1 - 1)/2w_1.$$

Proof. The variational matrix of system (4) about E_2 is

$$\begin{bmatrix} a_{11} & a_{12} \\ a_{21} & 0 \end{bmatrix}, \text{ where } a_{11} = x^*\left(-1 + \frac{w_1y^*}{(1 + w_1x^*)^2}\right); \quad a_{12} = -\frac{x^*}{(1 + w_1x^*)}; \quad a_{21} = y^*\left(\frac{w_3w_4y^*}{(1 + w_4x^*)^2}\right). \tag{6}$$

Its eigenvalues are given by

$$\lambda_{1,2} = \frac{1}{2}\left(a_{11} \pm i\sqrt{(4p - a_{11}^2)}\right), \quad p = -a_{12}a_{21} > 0. \tag{7}$$

Using $\mathrm{Re}(\lambda_{1,2}) < 0$,

Therefore, the equilibrium point E_2 is locally asymptotically stable in domain D' under the condition

$$x^* > (w_1 - 1)/2w_1. \quad \square \tag{8}$$

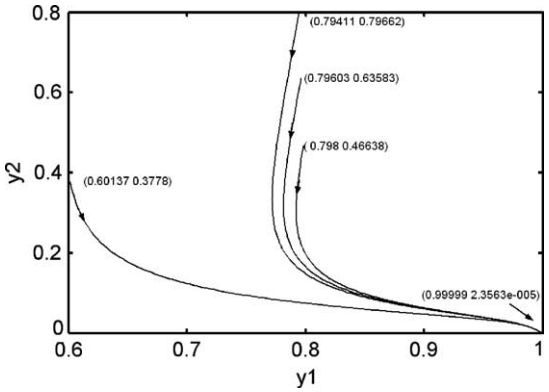

Fig. 1. Global stability at (1,0).

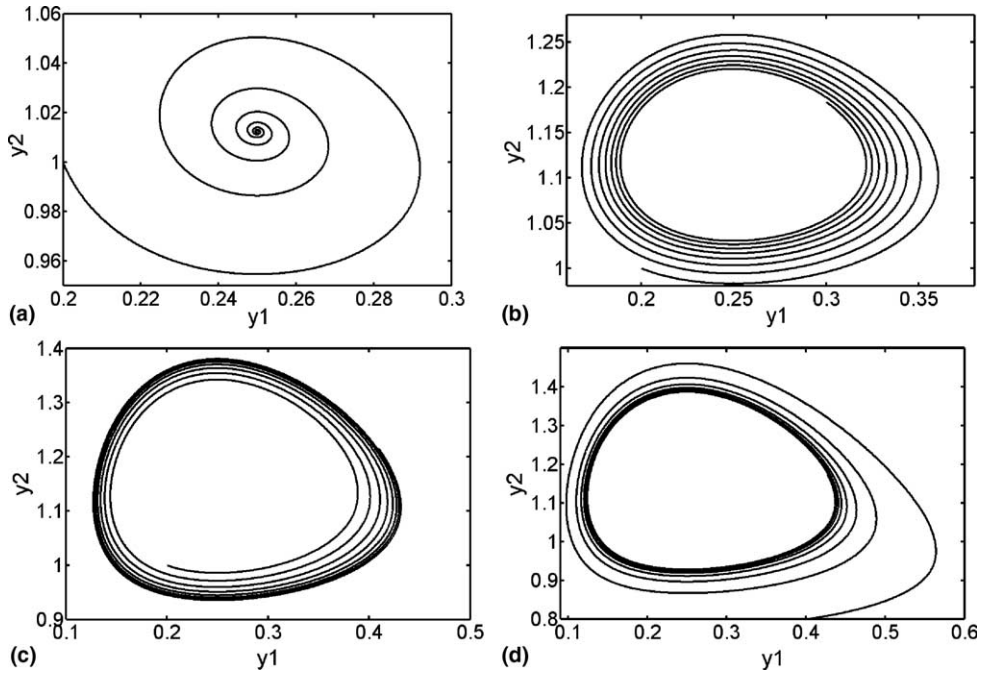

Fig. 2. Hopf bifurcation diagram. (a) Asymptotically stable at $w_1 = 1.4$; (b) Loss of stability at $w_1 = 2$; (c) Stable limit cycle at $w_1 = 2.2$ from inside; (d) Stable limit cycle at $w_1 = 2.2$ from outside.

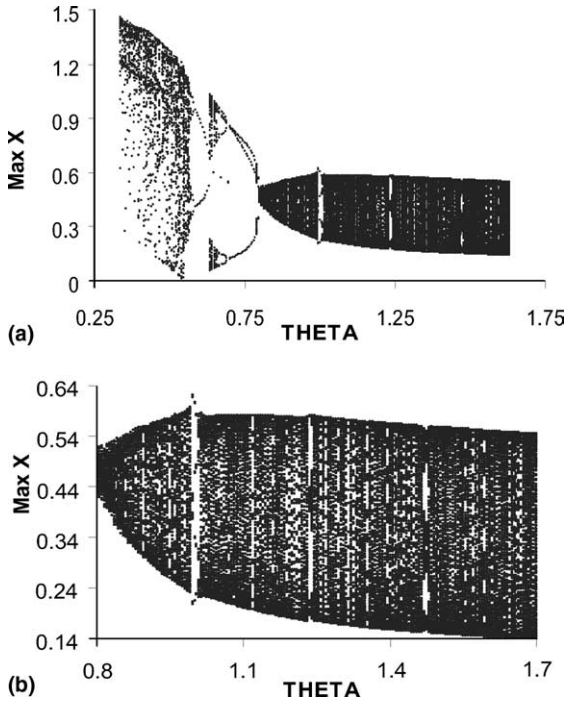

Fig. 3. The bifurcation diagram with respect to θ for $\phi = 0$.

Theorem 3.5. *Kolmogorov system (4) admits a stable limit cycle in domain D' provided following condition is satisfied*

$$x^* < (w_1 - 1)/2w_1. \tag{9}$$

Proof. Since by Theorem 3.4, the unique non-zero positive equilibrium point E_2 is locally asymptotically stable in domain $(w_1-1)/2w_1 < x^*$; therefore by Poincare–Bendixon criteria, there must be a limit cycle in region $0 < x^* < ((w_1-1)/2w_1)$.

Using (7), we get

$$\frac{\partial \mathrm{Re}(\lambda_{1,2})}{\partial w_1} = \frac{x^*(1-x^*)}{2(1+w_1x^*)^2} > 0 \quad \text{in domain} \quad 0 < x^* < ((w_1-1)/2w_1)$$

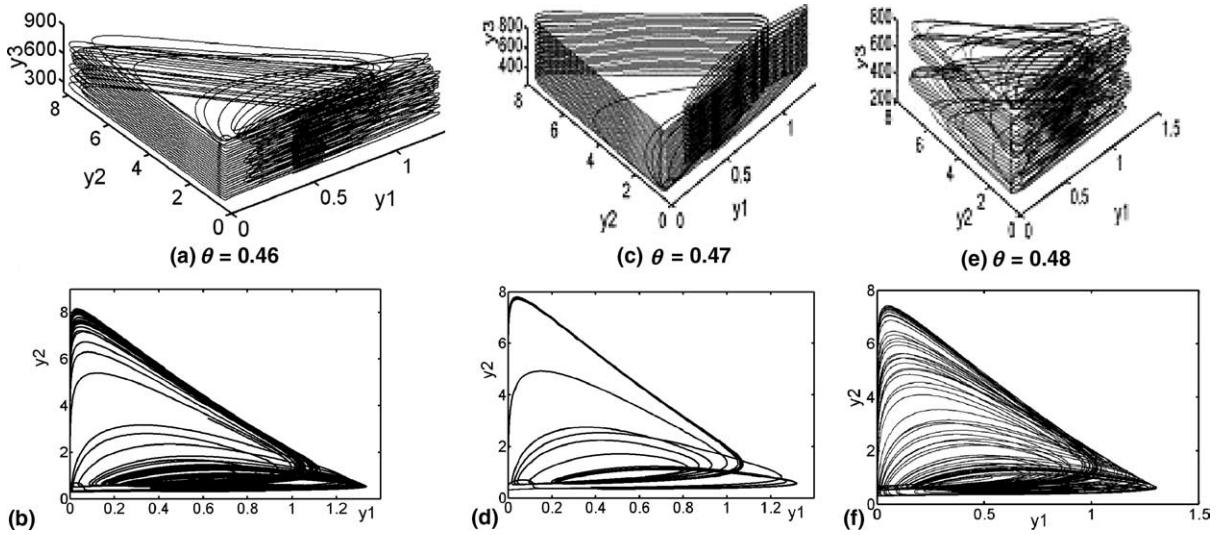

Fig. 4. Phase space trajectories and their projections in the region R_1 at $\phi = 0$.

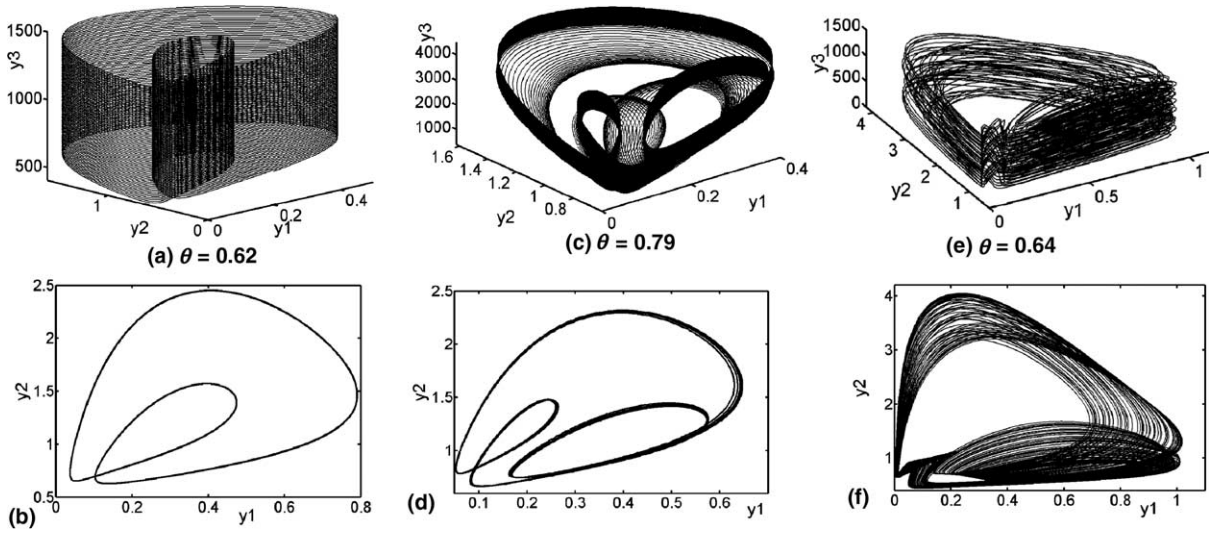

Fig. 5. Phase space trajectories and their projections in the region R_2 at $\phi = 0$.

and

$$\frac{\partial^2 \mathrm{Re}(\lambda_{1,2})}{\partial w_1^2} = -\frac{x^{*2}(1-x^*)}{(1+w_1x^*)^3} < 0 \quad \text{in domain } 0 < x^* < ((w_1-1)/2w_1).$$

Since $\frac{\partial \mathrm{Re}(\lambda_{1,2})}{\partial w_1} > 0$ and $\frac{\partial^2 \mathrm{Re}(\lambda_{1,2})}{\partial w_1^2} < 0$, therefore, Kolmogorov system (4) admits a stable limit cycle in domain D' [8]. □

Theorem 3.6. *The system admits a supercritical Hopf bifurcation in some region of the domain*

$$\{(x^*, y^*) : \ 0 < x^* < 0.5; \ y^* > 0\}.$$

Proof. The variational matrix will have purely imaginary roots $\lambda = \pm i\sqrt{p}$ for the condition

$$w_1^* = \frac{1}{(1-2x^*)} > 0 \Rightarrow 0 < x^* < 0.5. \tag{10}$$

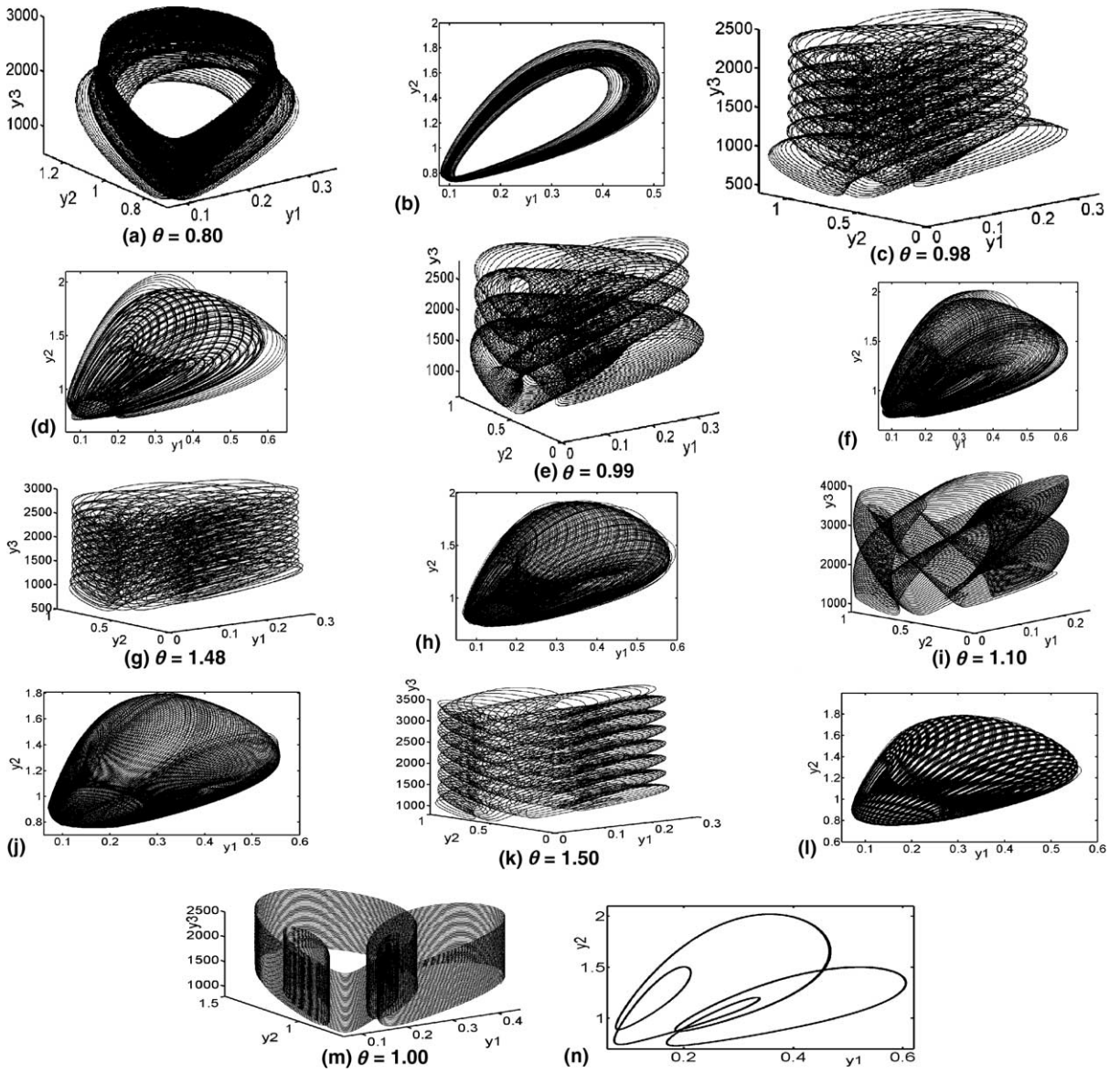

Fig. 6. Phase space trajectories and their projections in the region R_3 at $\phi = 0$.

As w_1 is increased the stationary solution loses stability. Note that $\mathrm{Re}(\lambda_{1,2}) < 0$ and

$$\frac{\partial \mathrm{Re}(\lambda_{1,2})}{\partial w_1} = \frac{x^*(1-x^*)}{2(1+w_1x^*)^2} = \frac{x^*(1-2x^*)^2}{2(1-x^*)} > 0 \text{ at } w_1^* \text{ in domain } 0 < x^* < 0.5. \tag{11}$$

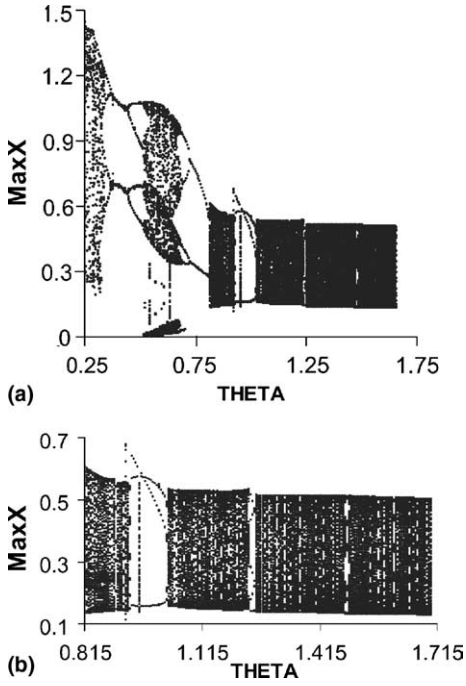

Fig. 7. Bifurcation diagrams with respect to θ for $\phi = \pi/2$.

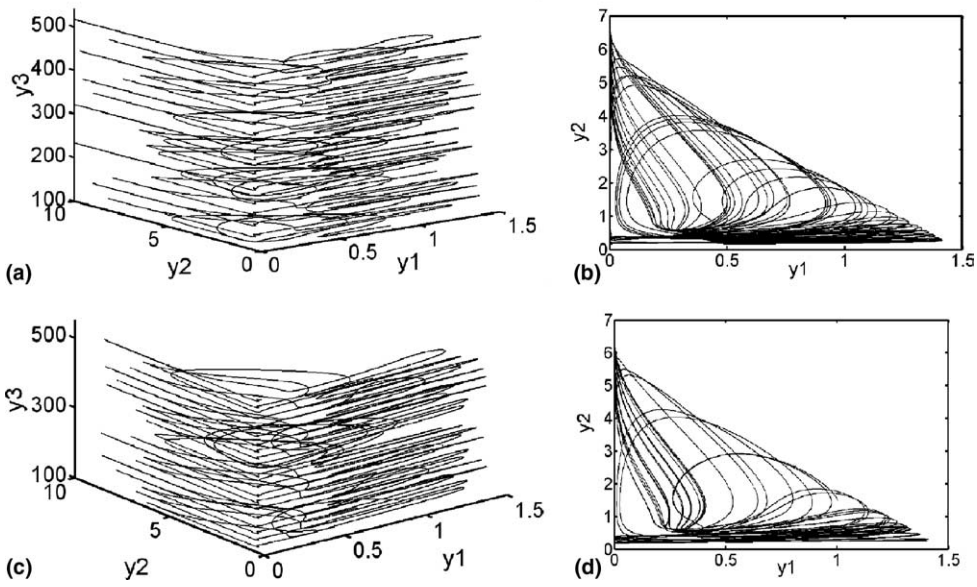

Fig. 8. Phase space trajectories and their projections in the region R_1' at $\phi = \pi/2$.

Therefore, the system admits a periodic solution of the amplitude $2\pi/|\lambda|$. As w_1 varies, the system (4) admits Hopf bifurcation at (10).

Using (10), we get

$$\frac{\partial a_{11}}{\partial w_1}+\frac{\partial a_{22}}{\partial w_1}=\frac{x^*y^*(1-3x^*)}{(1+w_1^*x^*)^3(1-2x^*)}>0.$$

Consider

$$a=\frac{1}{16}\left[\left(\frac{\partial^2 a_{11}}{\partial x^2}+\frac{\partial^2 a_{22}}{\partial x^2}+\frac{\partial^2 a_{12}}{\partial x\partial y}\frac{\partial^2 a_{22}}{\partial y^2}\right)+\frac{1}{\omega}\left(\frac{\partial a_{12}}{\partial x}\left(\frac{\partial a_{11}}{\partial x}+\frac{\partial a_{12}}{\partial y}\right)-\frac{\partial a_{22}}{\partial x}\left(\frac{\partial a_{21}}{\partial x}+\frac{\partial a_{22}}{\partial y}\right)-\frac{\partial a_{11}}{\partial x}\frac{\partial a_{21}}{\partial x}+\frac{\partial a_{12}}{\partial y}\frac{\partial a_{22}}{\partial y}\right)\right].$$

Substituting the values in the above expression [9] and simplifying, we get

$$a=\frac{1}{16}\left[\frac{\partial^2 a_{11}}{\partial x^2}+\frac{1}{\omega}\frac{\partial a_{11}}{\partial x}\left(\frac{\partial a_{12}}{\partial x}-\frac{\partial a_{21}}{\partial X}\right)\right]=-\frac{(p_1+p_2)}{16(1+w_1x^*)^2},$$

where

$$p_1=\frac{2dw_3w_4^2y^{*2}}{(1+w_4x^*)^3};\quad p_2=\frac{1}{\omega}\left(\frac{2(1-x^*)}{(1+w_1^*x^*)^2(1-2x^*)^4}f(x^*)\right);\quad d=\frac{2x^*(1-x^*)}{\omega(1-2x^*)^2}>0;$$
$$f(x^*)=\{2\omega-x^*(7\omega+1)+x^{*2}(5\omega+4)-4x^{*3}\};\ \omega=\sqrt{p}.\qquad\square$$

Since $f(0)=2\omega>0$ and $f(0.5)=-\omega/4<0$, there exists a subinterval of $0<x^*<0.5$ for which $f(x^*)>0$. Therefore, p_1 and p_2 being positive, $a<0$ in some subinterval. Further, $a\left(\frac{\partial a_{11}}{\partial w_1}+\frac{\partial a_{22}}{\partial w_1}\right)=-\left(\frac{1}{16(1+w_1x^*)^2}(p_1+p_2)\right)\left(\frac{x^*y^*(1-3x^*)}{(1+w_1^*x^*)^3(1-2x^*)}\right)<0$ at w_1^* obtained from (10).

Thus, by Hopf's theorem [9] positive non-zero equilibrium must be unstable and the limit cycle solution must be stable in the Kolmogorov system.

For the choice of parameter values $w_2=0.2$, $w_3=0.3$, $w_4=2$, the analysis suggests that the Hopf bifurcation occurs at $w_1=2$. The numerical simulations in Fig. 2 shows the asymptotically stability at $w_1=1.4$ (see Fig. 2a). Fig. 1b shows

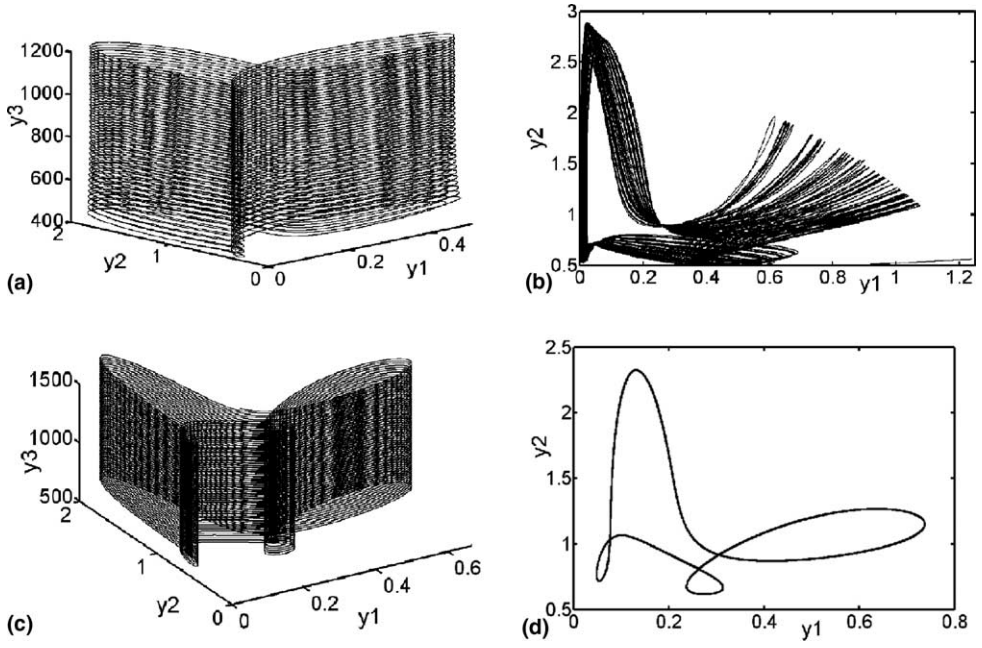

Fig. 9. Phase space trajectories and their projections in the region at R_2' at $\phi=\pi/2$.

the loss of stability at the bifurcation point $w_1 = 2$. The existence of stable limit cycle from inside as well as outside at $w_1 = 2.2$ is shown in (c) and (d) for different initial conditions.

4. Results of numeric simulations of forced system

To study the global dynamics of the prey–predator system (3) with seasonally varying parameters, the numerical solutions of the system with initial conditions in the first octant are obtained for time $t = nh$, h being the step size and n having a large integral value representing the number of steps. The selection of parametric values in the domain where the unforced system is Kolmogorov ensures the biological feasibility of the system. The system being nonlinear and three-dimensional, variety of behavior in the solution are expected in contrast to the corresponding two-dimensional system without seasonality. The term "bifurcation" refers to significant changes in the stability of fixed point or periodic orbits or other sets of interest. Since, the bifurcation diagram provides a summary of essential dynamical behavior of the system, the bifurcation diagrams are drawn for different key parameters. In the bifurcation diagram, after removing the transient effects in the solution, the local maximum values of predator species X is plotted for a range of the key parameter. The key parameters are identified as θ and w_4. The bifurcation diagrams are drawn with respect to

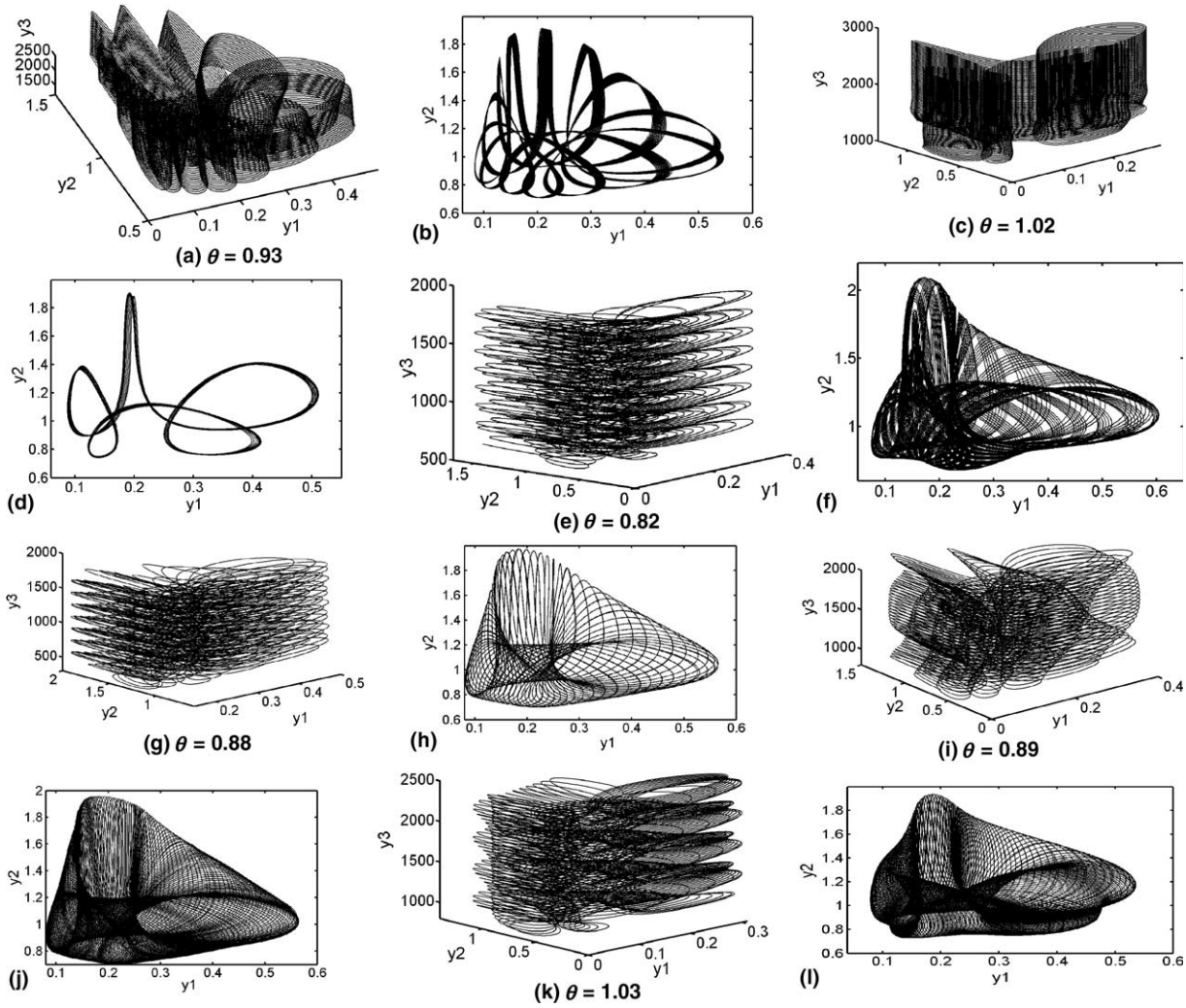

Fig. 10. Phase space trajectories and their projections in the region R_3' at $\phi = \frac{\pi}{2}$.

these parameters in the three cases, viz. $\phi = 0$, $\pi/2$ and π. The case $\phi = 0$ corresponds to the synchronous seasonal variations. We have taken initial condition as (0.1, 0.03, 0.0).

The bifurcation diagrams shown in Fig. 3 are drawn with respect to θ for the following choice of parameters:

$$w_1 = 2.0, \quad w_2 = 0.3, \quad w_3 = 0.4, \quad w_4 = 1.5, \quad \epsilon_1 = 0.5, \quad \lambda = 0.27, \quad 0.25 \leqslant \theta \leqslant 1.7. \tag{12}$$

From Fig. 3(a), it is observed that the behavior of solution is categorized in three regions for $\phi = 0$:

(i) $R_1 = \{\theta : \theta \in (0.335, 0.57)\}$: The solution is chaotic in this region.
(ii) $R_2 = \{\theta : \theta \in (0.57, 0.80)\}$: After repeated period halving, period-$2T$ solution is obtained. In a narrow region $\{\theta : \theta \in (0.635, 0.665)\}$ solution again becomes chaotic. After a series of period halving, the solution becomes periodic of period $4T$ and later on of period $2T$.
(iii) $R_3 = \{\theta : \theta \in (0.8, 1.7)\}$: The solution alternates randomly between regular periodic solutions and irregular bursts in this region. The blow up of this region in Fig. 3(b) supports this fact. Typical phase space trajectories and their projections in the phase plane are drawn in Fig. 4. In Fig. 4(a) and (b) the chaotic behaviors is shown for $\theta = 0.46$. For nearby values of $\theta = 0.47$ and 0.48 in the region, different phase space and their projections are obtained as in Fig. 4(c)–(f). These are found to be sensitive to initial conditions.

In region (ii), the phase space trajectories and their projections are drawn in Fig. 5. After removing transient effects, the phase space and their projections in Fig. 5(a) and (b) for $\theta = 0.62$ shows oscillations of $2T$ period in phase plane and the quasiperiodic in cylindrical form in phase space. As θ changes the shape of the phase space and their projections also changes. A different type phase space and their projection is shown in Fig. 5(c) and (d) at $\theta = 0.79$. In a narrow chaotic region, phase space solution is drawn for $\theta = 0.64$ in Fig. 5(e). It is found to be sensitive to initial conditions and chaotic. Its corresponding projection in phase plane is drawn in Fig. 5(f).

In the region (iii), we get different type phase space trajectories and their projections for $\theta = 0.80$, 0.98, 0.99, 1.10, 1.48, and 1.50 as shown in Fig. 6(a)–(l). These are again found to be sensitive to initial values. However, the phase space and their projections for $\theta = 1.0$ in Fig. 6(m), 6(n) shows quasiperiodic in phase space and period doubling in phase plane.

The bifurcation diagrams in Fig. 7(a) are drawn for the above set of data with $\phi = \pi/2$. It is observed that the behavior is again classified into three regions. However the first region $R_1' = \{\theta : \theta \in (0.25, 0.335)\}$ is shifted to the left and reduced in size as compared to$\phi = 0$. The third region is also shifted to the left side. The behavior in the second region $R_2' = \{\theta : \theta \in (0.335, 0.815)\}$ is quite different in this case. Initially the solution becomes periodic of period $2T$. But soon chaos sets in through period doubling route. The chaotic region is more pronounced. Repeated period halving takes

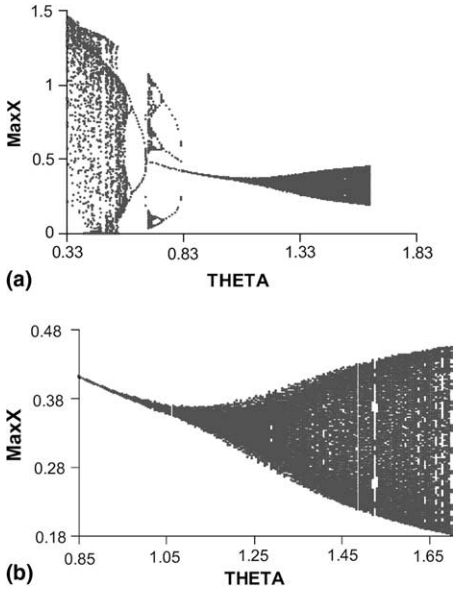

Fig. 11. Bifurcation diagrams with respect to θ for $\phi = \pi$.

place and the solution becomes periodic of period $2T$. In third region $R_3' = \{\theta : \theta \in (0.815, 1.7)\}$ the behavior is found to be chaotic. Fig. 7(b) shows the blown up bifurcation diagram in this region.

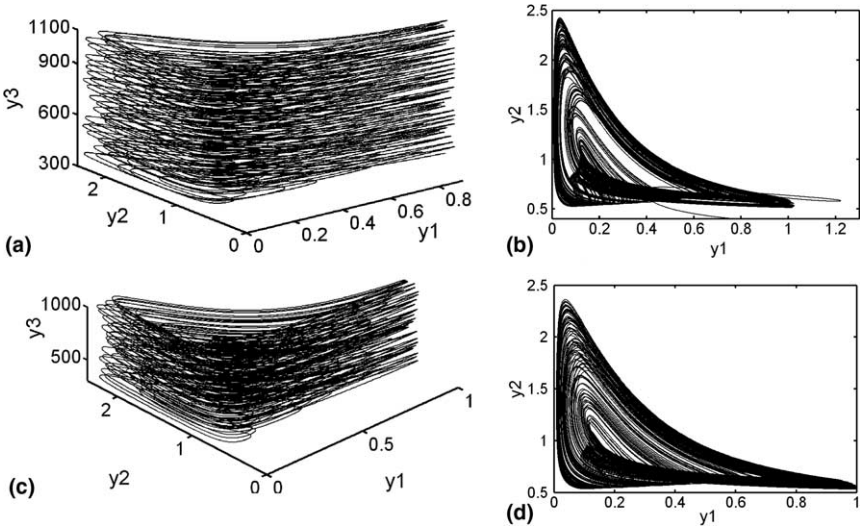

Fig. 12. Phase space trajectories and their projections in the region R_1'' at $\phi = \pi$.

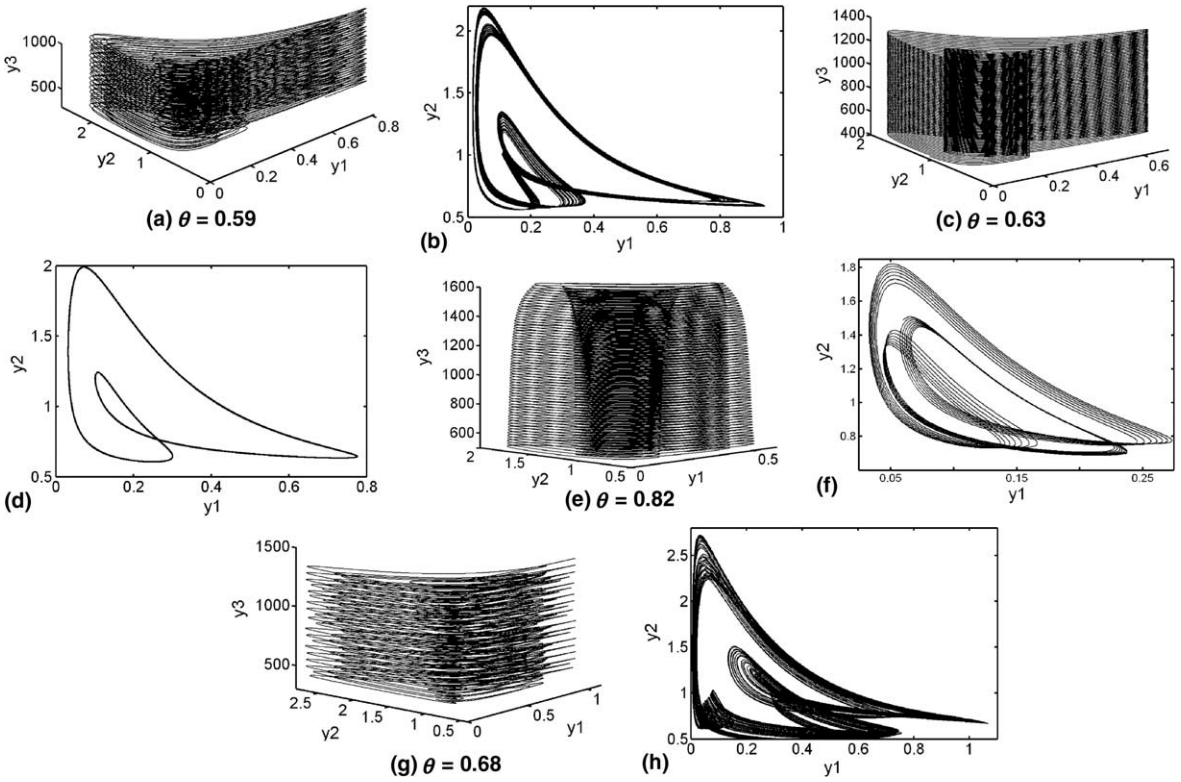

Fig. 13. Phase space trajectories and their projections in the region R_2'' at $\phi = \pi$.

In the region (i), the phase space trajectories and their projections are drawn in Fig. 8. The phase space and their projections in Fig. 8(a)–(d) are drawn for nearby points $\theta = 0.26$, 0.27. They are sensitive to initial values and are chaotic.

In the region (ii), the phase space trajectories and their projections are drawn in Fig. 9. The phase space and their projections for $\theta = 0.56$ in Fig. 9(a) and (b) show the non-chaotic behavior. However, in Fig. 9(c) and (d) shows quasiperiodic in phase space and a periodic solution of period $4T$ in phase plane. These phase spaces and their projections are different than those for $\phi = 0$.

In the region (iii), the phase space trajectories and their projections are drawn in Fig. 10. The phase space and their projections for $\theta = 0.82$, 0.88, 0.89, 1.03 in Fig. 10(e)–(l) are distinct and they are sensitive to initial values. However, in Fig. 10(a)–(d) for $\theta = 0.93$ and 1.02, respectively, the phase space and their projections are periodic with multiplicity more than $4T$ in phase plane and quasiperiodic in phase space.

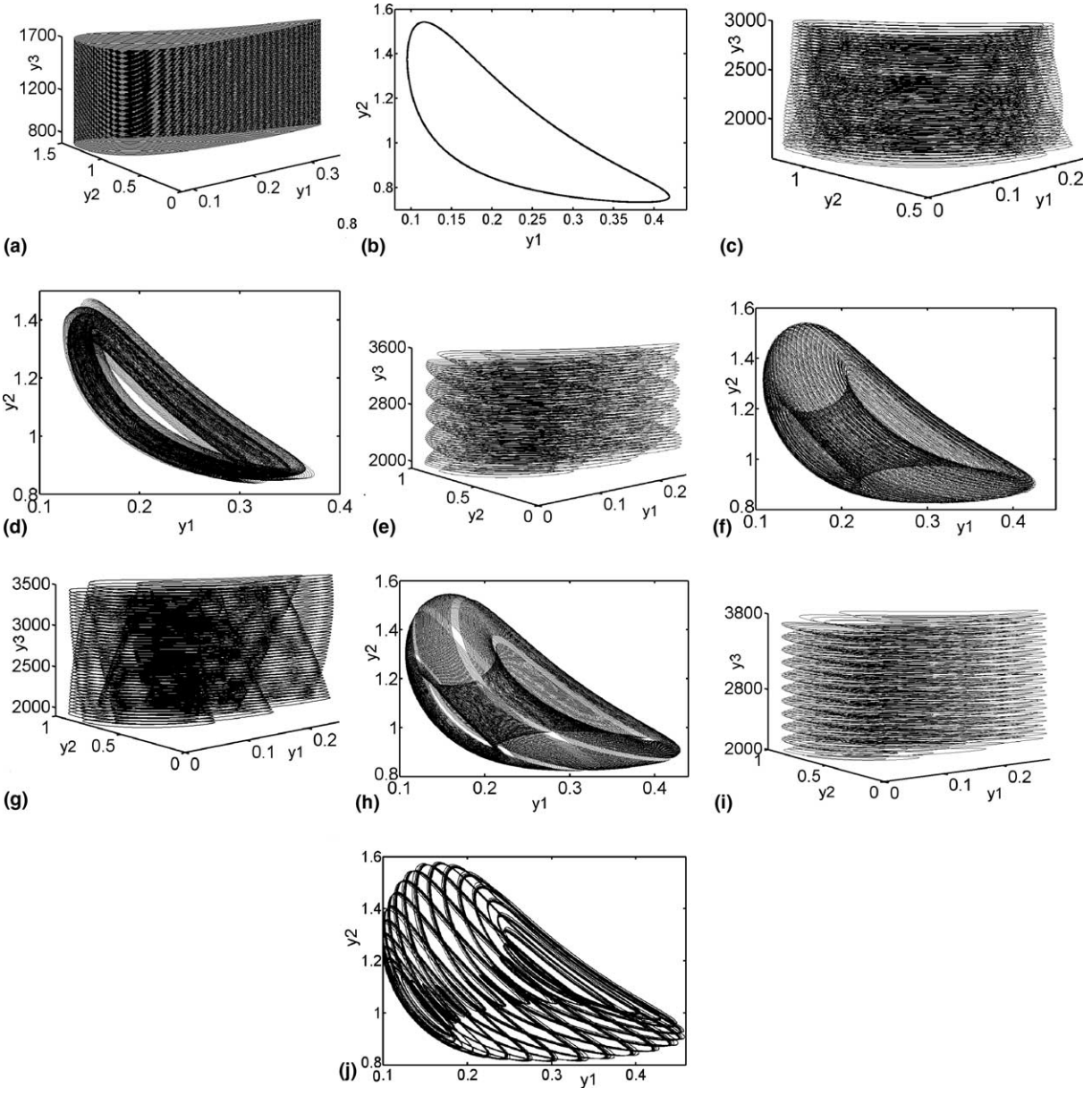

Fig. 14. Phase space trajectories and their projections in the region R_3'' at $\Phi = \pi$.

The bifurcation diagrams in Fig. 11(a) and (b) are drawn for the above set of data with $\phi = \pi$. It is observed that the behavior is again classified into three regions. The first region $R_1'' = \{\theta : \theta \in (0.335, 0.59)\}$ is reduced in size. The behav-

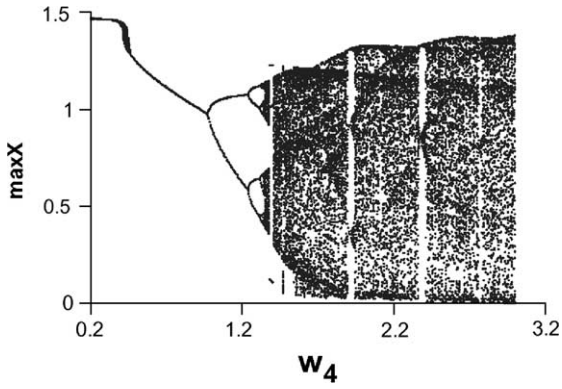

Fig. 15. Bifurcation diagram with respect to w_4 for $\phi = 0$.

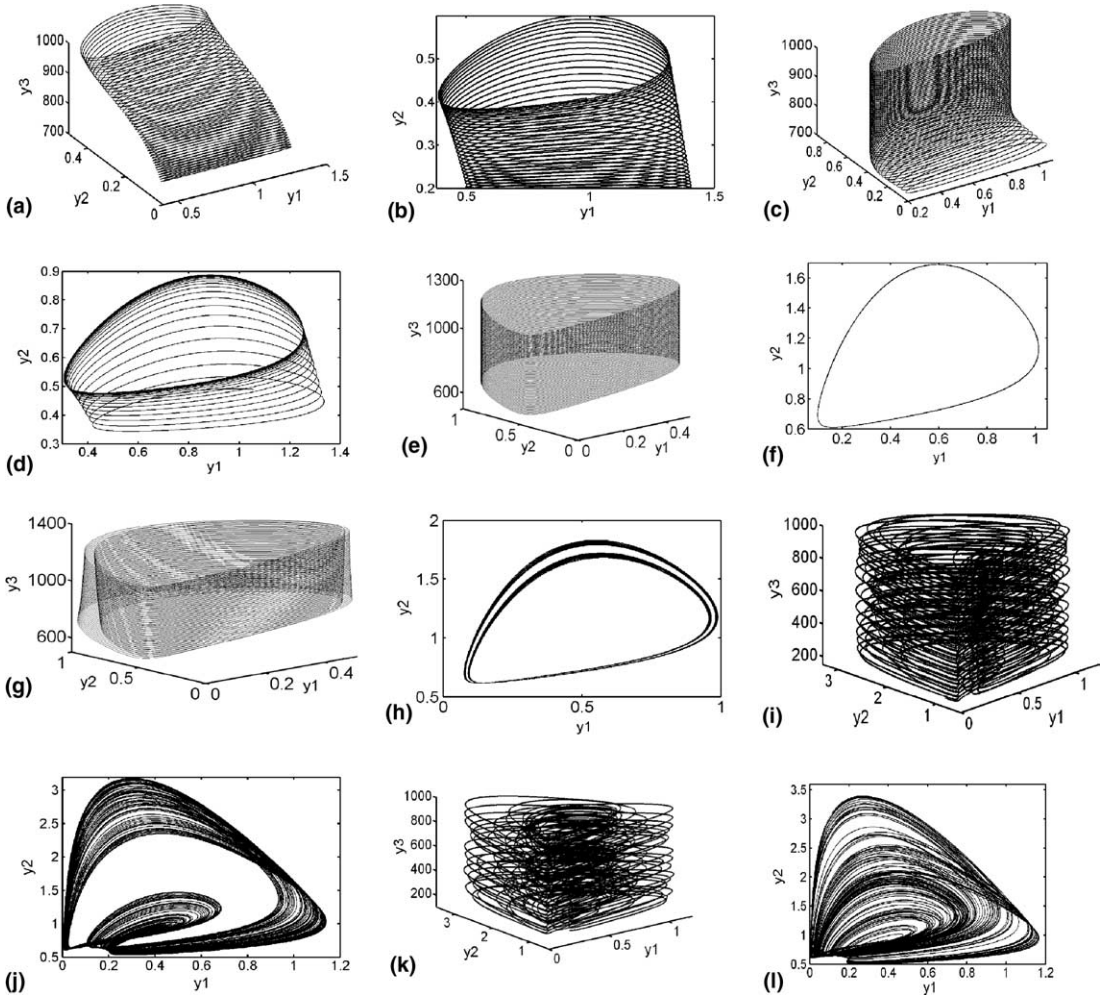

Fig. 16. Phase space trajectories and their projections at $\phi = 0$.

ior in the second region $R_2'' = \{\theta : \theta \in (0.59, 0.82)\}$ is different. Initially, the solution becomes periodic from period $4T$ to period T. But soon chaos sets in through period doubling route. The chaotic region is more pronounced. Repeated period halving takes place and the solution becomes periodic of period one and later becomes chaotic in third region $R_3'' = \{\theta : \theta \in (0.82, 1.7)\}$.

In the region (i), the phase space trajectories and their projections are drawn in Fig. 12. The nearby phase space and their projections for $\theta = 0.56, 0.57$ in Fig. 12(a)–(c) are chaotic and sensitive to initial values, which are of same type.

In the region (ii), the phase space trajectories and their projections are drawn in Fig. 13. The phase space and their projections for $\theta = 0.63, 0.82$ in Fig. 13(c), (e) and (d), (f) shows period doubling in phase plane and quasiperiodic in phase space. The attractors for $\theta = 0.59$ and $\theta = 0.68$ in Fig. 13(a) and (g) are chaotic and are sensitive to initial values in narrow chaotic region.

In the region (iii), the phase space trajectories and their projections are drawn in Fig. 14. The phase space and their projections for $\theta = 0.83$ in Fig. 14(a) and (b) show the stable periodic solution in phase plane and quasiperiodic in phase space after removing the transients effect. The phase space and their projections for $\theta = 1.3, 1.5, 1.53, 1.7$ in Fig. 14(c)–(j) are chaotic and are sensitive to initial value.

We next assume the critical parameter as w_4. Figs. 15, 17 and 19 show the bifurcation diagrams for $\phi = 0$, $\pi/2$ and π as a function of w_4 in the range $0.20 \leqslant w_4 \leqslant 3$, while other parameters being fixed as

$$w_1 = 2.0, \quad w_2 = 0.3, \quad w_3 = 0.4, \quad w_4 = 0.20, \quad \epsilon_1 = 0.5, \quad \lambda = 0.2, \quad \theta = 0.5. \tag{13}$$

From Fig. 15, the evidence for cascade of periodic doubling leading to chaos can be seen clearly for $1.345 \leqslant w_4 \leqslant 3.0$. The solution becomes chaotic for $w_4 \geqslant 1.345$. There are number of periodic windows in this region. The more pronounced windows occur at $1.38 \leqslant w_4 \leqslant 1.41$; $1.465 \leqslant w_4 \leqslant 1.48$; $1.895 \leqslant w_4 \leqslant 1.945$; $2.365 \leqslant w_4 \leqslant 2.415$; $2.76 \leqslant w_4 \leqslant 2.79$. In the interval [0.21, 0.465], Fig. 15 shows the quasiperiodic solution. Solution is periodic in the region (0.465, 0.98]. Repeated periodic doubling takes place in the interval (0.98, 1.33] and it becomes chaotic in the region (1.33, 3.0]. Periodic windows are also visible in this region.

Some phase space trajectories and their projections are shown in Fig. 16. The quasiperiodic attractor in phase space and its projection are shown in Fig. 16(a) and (b), respectively, at $w_4 = 0.44$. The similar behavior is obtained at $w_4 = 0.49$ and $w_4 = 0.89$ in Fig. 16(e)–(f). The phase space attractor and its projection in Fig. 16(g) and (h) at $w_4 = 0.975$ shows the period doubling in phase plane and quasiperiodic in cylindrical form in phase space on removing

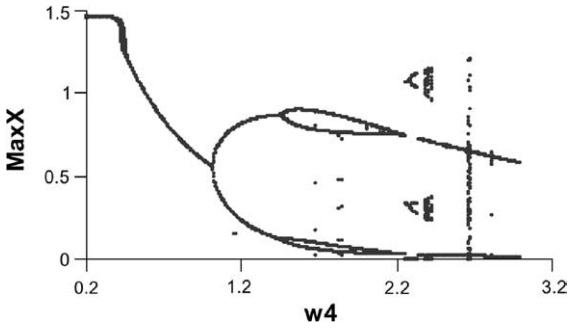

Fig. 17. Bifurcation diagram with respect to w_4 for $\phi = \frac{\pi}{2}$.

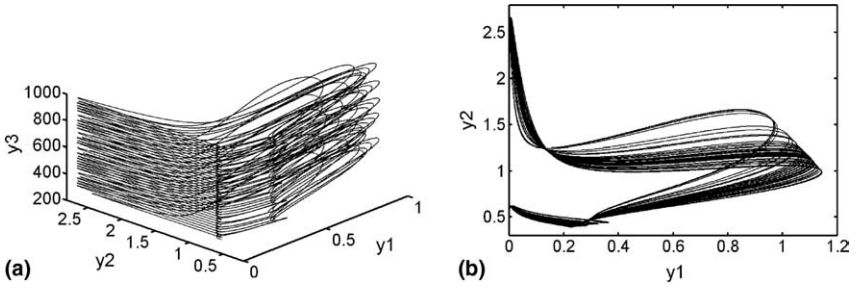

Fig. 18. Phase space trajectory and its projection for $w_4 = 2.41$ at $\phi = \frac{\pi}{2}$.

the transient effect. The phase space attractors and their projections in Fig. 16(i)–(l) at $w_4 = 1.37$, $w_4 = 1.44$ are found to be chaotic.

Fig. 17 is drawn for $\phi = \pi/2$. It is observed that the solution is quasiperiodic in the interval [0.21, 0.47]. Stable periodic solution is evident in the interval (0.47, 1.02]. It is further observed that the region of chaotic activity in the region (1.02, 3.0] is reduced. Chaotic attractor in phase space and its projection is drawn in Fig. 18.

However, for the $\phi = \pi$, the chaotic region again becomes denser. Fig. 19 shows the quasiperiodic nature of the solution in the interval [0.21, 0.47]. Stable periodic solution exists in the interval (0.47, 0.96]. After a cascade of period doubling the solution becomes chaotic in the interval (1.24, 3.0]. The periodic windows are visible but they are narrower as compared to the case $\phi = 0$.

The phase space trajectories in Fig. 20(a) and (c) show the quasiperiodic nature of the solution at $w_4 = 0.96$ and $w_4 = 1.1$ respectively. However, Fig. 20(b) and (d) shows the asymmetrical period doubling in phase plane. Further,

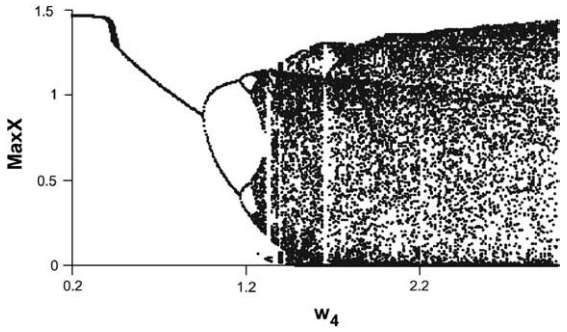

Fig. 19. Bifurcation diagram with respect to w_4 for $\phi = \pi$.

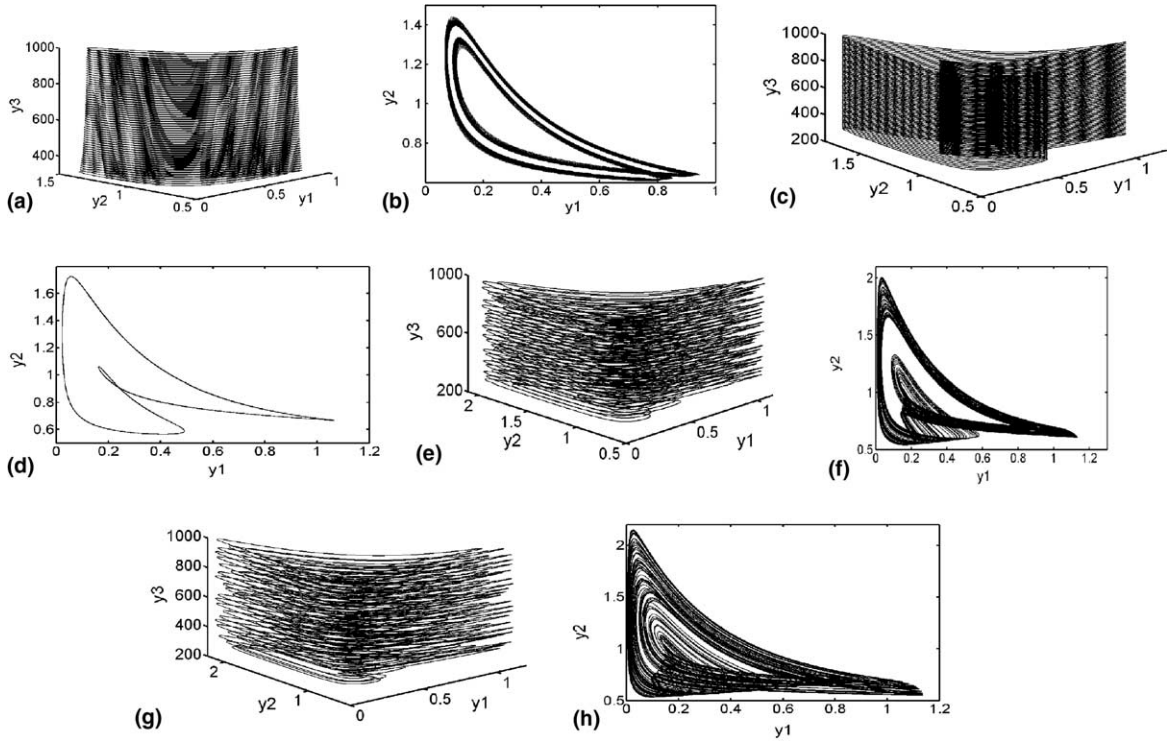

Fig. 20. Phase space trajectories and their projections at $\phi = \pi$.

for $w_4 = 1.29$ and 1.38 the chaotic attractors are obtained in Fig. 20(e) and (g), respectively. Their projections are drawn in Fig. 20(f) and (h). These bifurcation diagrams are found to be sensitive to initial conditions in all cases.

5. Conclusion

In this paper, we have considered the model consisting of the modified Leslie–Gower predator with logistic prey species. We have investigated the co-existence in the form of periodic solutions and global stability of $(1,0)$ equilibrium by using the Liapunov's direct method. Supercritical Hopf's bifurcation has been investigated in respect of the key parameter w_1, which provides the information about the instability region near the positive non-zero equilibrium point. Besides above these, the chaotic dynamics is found in the nonlinear non-autonomous two-dimensional ordinary differential system by taking the seasonal effect in the intrinsic growth of prey as well as predator species.

References

[1] Rinaldi S, Muratori S, Kuznetsov AYu. Multiple attractors, catastrophes and chaos in seasonally perturbed predator–prey communities. Bull Math Biol 1993;55:15–35.
[2] Sabin GCW, Summer D. Chaos in a periodically forced predator–prey ecosystem model. Math Biosci 1993;113:91–113.
[3] Moghadas SM, Alexander ME. Dynamics of a generalized Gause-type predator–prey model with a seasonal functional response. Chaos, Solitons & Fractals 2005;23:55–65.
[4] Gakkhar S, Naji RK. Seasonally perturbed predator–prey system with predator-dependent functional response. Chaos, Solitons & Fractals 2003;18:1075–83.
[5] Aziz-Alaoui MA. Study of a Leslie–Gower-type tri-trophic population model. Chaos, Solitons & Fractals 2002;14:1275–93.
[6] Gakkhar S, Singh B. Complex dynamics in a food web consisting of two preys and a predator. Chaos, Solitons & Fractals 2005;24:789–801.
[7] Freedman HI. Deterministic mathematical models in population ecology. New York, USA: Marcal Dekker, Inc.; 1980.
[8] Moiola Jorge L, Chen G. Hopf bifurcation analysis. Singapore: World Scientific; 1996.
[9] Lakshmanan M, Rajasekar S. Nonlinear Dynamics. Berlin: Springer-Verlag; 2003.